Research article

Dan Zhang[a], Chenxi Zhang[a], Xiaohui Li* and Abdul Qyyum

Layered iron pyrite for ultrafast photonics application

https://doi.org/10.1515/nanoph-2020-0014
Received January 10, 2020; revised February 19, 2020; accepted February 23, 2020

Abstract: Two-dimensional (2D) transition metal dichalcogenide materials have attracted much attention in recent years due to their excellent electro-optical properties. FeS_2, the ideal composition of iron pyrite, is a 2D transition metal dichalcogenide which has been potentially used in the electronic, optical, and chemical fields. On the other hand, the narrow band gap of FeS_2 (≈0.96 eV) makes it very suitable and promising for the ultrafast application in near-infrared regimes. However, the potential application of FeS_2 in laser technology has not been explored till now. Ultrashort pulse lasers have great applications in industry and science because of its stability, ease of operation, and portability. Passively mode-locked fiber lasers using 2D materials (such as MoS_2, CuS_2, and WS_2) as saturable absorber are intensively investigated. Here, layered FeS_2 has been characterized systematically. It is successfully applied in ultrafast photonics and plays a key component in the passively mode-locked laser for the first time. The single pulse can be obtained with 1.7-ps pulse duration, 1.89-nm spectral width, and fundamental repetition of 6.4 MHz at 1563 nm central wavelength. Through controlling the pump power, the evolution of the pulse train can be observed, which can be transformed from single pulse to bound states. Also, the harmonic mode-locked fiber laser is observed with the pump power high enough.

Keywords: iron pyrite; ultrafast photonics; transition metal dichalcogenide; 2D materials.

1 Introduction

Low-dimensional materials have attracted increasing attention in nonlinear optics due to their remarkable optoelectronic properties. For instance, one-dimensional carbon nanotubes (CNTs) and two-dimensional (2D) graphene were found to possess ultrafast carrier dynamics and high third-order nonlinear susceptibility [1–9]. Over the past decade, 2D materials have been widely reported in nonlinear optics, ultrafast photonics, and other fields due to their energy band structure and splendid crystals [10–13]. Up to now, a considerable number of experiments have demonstrated that the optical nonlinearity of 2D nanomaterials is enhanced without sacrificing ultrafast response. Transition metal dichalcogenides (TMDs) are a kind of highly anisotropic layered semiconductor materials which attract growing research attention due to their excellent physical/chemical properties. The chemical formula is MX_2, where M represents the transition metal (commonly Mo, W) and X represents a group VI element (S, Se, Te). Each TMD monolayer is composed of two hexagonal planes of X atoms and an intermediate hexagonal plane of M atoms. The M atoms are coordinated by covalent bonds with the X atoms in a trigonal prismatic arrangement. They offer further optoelectronic opportunities and result in the advancement of fascinating applications such as optical switches, photo detectors, and quantum well modulators due to their unique thickness-dependent band gap. In addition, they submit to a transition from an indirect band gap in bulk to a direct band gap in the monatomic layer [14]. Compared with graphene, TMDs such as molybdenum disulfide (MoS_2) [15–18] and tungsten disulfide (WS_2) exhibit distinct and complementary properties. For example, the field-effect transistors made of TMDs single layer possess high mobility and large on/off ratio. Much more effort is needed to promote their practical applications. Earth abundance and non-toxicity pyrite

[a]**Dan Zhang and Chenxi Zhang:** These authors contributed equally to this work.
***Corresponding author: Xiaohui Li,** College of Physics and Information Technology, Shaanxi Normal University, Xi'an, Shaanxi, 710119, P.R. China, e-mail: lixiaohui0523@163.com. https://orcid.org/0000-0002-5600-3820
Dan Zhang: School of Physics and Information Technology, Shaanxi Normal University, Xi'an, China; and College of Science, Northwest A and F University, Yangling 712100, P.R. China
Chenxi Zhang and Abdul Qyyum: School of Physics and Information Technology, Shaanxi Normal University, Xi'an, China

Open Access. © 2020 Xiaohui Li et al., published by De Gruyter. This work is licensed under the Creative Commons Attribution 4.0 Public License.

iron disulfide (FeS_2) as one kind of TMD is widely used in basic and applied research. It is a potential candidate to be applied for wide-range nonlinear photonics because of its large optical absorption coefficient (>105 cm^{-1}) and narrow band gap 0.95 eV [19–21]. Alivisatos et al. have compared all the 23 kinds of inorganic semiconductor materials and obtained the following conclusion: FeS_2 is the material with the lowest cost and the highest power supplement [22]. For example, with the photovoltaic conversion efficiency up to 4%, its power supply capacity is 100 times that of a monocrystalline silicon cell. FeS_2 is considered to be an excellent electrode material candidate for energy storage devices. At present, research on FeS_2 at home and abroad mainly focuses on solar-cell materials and electronic properties [23–26].

Passive mode locking is still the most prominent technique to produce all kinds of ultrashort laser pulses [27–32]. Saturable absorber (SA) has been widely studied because of its lower cost and convenient preparation and used in the fiber laser cavity to act as an internal loss modulator [33–35]. With the development of the laser technology, high-performance fiber lasers and high-quality ultrashort laser pulse become more reliable and practical. SA made of various materials has been emerging, such as CNTs, black phosphorus, and graphene [36]. Materials with low band gap and layered structure are widely used as SA in fiber lasers especially TMDs (such as CuS_2, SnS_2, MoS_2, WS_2, etc.). Although FeS_2 has a layered structure and low band gap, its properties of ultrafast photonics have not been investigated yet.

In this paper, we demonstrate that FeS_2 exhibits SA property and can be used as SAs of ultrafast laser. The performances of FeS_2 are further tested in erbium-doped fiber lasers (EDFL), in which the width of the pulse is about 1.7 ps and the signal-to-noise ratio (SNR) is about 72 dB. It is observed that under appropriate phases and pump power, two or more solitons form in the fiber lasers and bind together to form bound states of solitons. It is demonstrated that the FeS_2 can be a potential candidate photonics material for ultrafast pulse generations.

2 Preparation and characterization of FeS_2

The synthetic procedure for the fabrication of FeS_2 is illustrated in Figure 1A. First, 15.781-g $FeSO_4 \cdot 7H_2O$ was completely dissolved in 100 mL distilled water to get aqueous solution A, and 10.482-g $Na_2S_2O_3 \cdot 5H_2O$ was dissolved in 100-mL distilled water to prepare an aqueous solution B. Solutions A and B were mixed up at room temperature in a beaker and stirred for 1 h. Then, we transferred the mixed solution into a teflon-lined stainless autoclave and heat it for 8 h with the temperature maintained at 180°C. It is then cooled to room temperature to obtain a black precipitate. Finally, we rinse the precipitate three times with deionized water and absolute ethanol and dry it in vacuum at 80°C for 8 h to get FeS_2 powder. $FeSO_4$ will react with $Na_2S_2O_3$ and form FeS_2 product under the hydrothermal conditions according to the following reaction:

$$2Na_2S_2O_3 + 2H_2O + FeSO_4 \rightarrow 2Na_2SO_4 + H_2SO_4 + FeS_2 + H_2$$

When we use FeS_2 in the fiber laser, we should mix up the FeS_2 powder with alcohol with a ratio of 1:2 for dispersion to form a stable suspension liquid. Before dropping the FeS_2 dispersible solution, oscillate for 40 min in the ultrasonic generator to fully disperse the FeS_2 solution. The photographs of the FeS_2 powder in a sealing bag and the FeS_2 suspension in a bottle are shown in Figure 1A from which we can see that the color of FeS_2 solution is dark grey.

The scanning electron microscopy (SEM) images of the FeS_2 dispersion at 5 μm and 500 nm scales are provided in Figure 1B and C which show that the FeS_2 have a few layers. The atomic structure of FeS_2 is shown in Figure 1D in which the local coordination of the iron atoms is sixfold and that of the sulfur atoms is fourfold. Figure 1E shows the energy dispersive spectrometer (EDS) analysis results of UV-Vis-NIR absorption of the layered FeS_2 dispersion, indicating that our material is mainly composed of 27.79% Fe and 46.62% S, and Si and Al are sample placement stations of SEM mechanism. This result is consistent with the atomic structure of FeS_2. Figure 1F is the high-resolution X-ray diffraction (HRXRD) diagram of FeS_2 microfilm dispersion and gives the direction indicators and proportions of each. There are nine peaks of intensity; the highest one is caused by an orientation index of (109). The Raman spectrum of FeS_2 dispersion is shown in Figure 1G. Different bands represent different properties of FeS_2. Six Raman bonds were observed at 208 cm^{-1} (corresponding to distance of the sulfur atom perpendicular to the S-S bond), 274 cm^{-1} (weak bonds), 386 cm^{-1} (due to in-phase S-S stretched vibration FeS_2), 580 cm^{-1} (weak bonds), 1096 cm^{-1} (weak bonds), and 1316 cm^{-1} (weak bonds). These above peaks show the cubic structure of FeS_2. The UV–Vis-Nir absorption spectrum of FeS_2 powder is shown in Figure 1H. The absorption of FeS_2 between 200 and 2000 nm is always larger than 75% which indicates

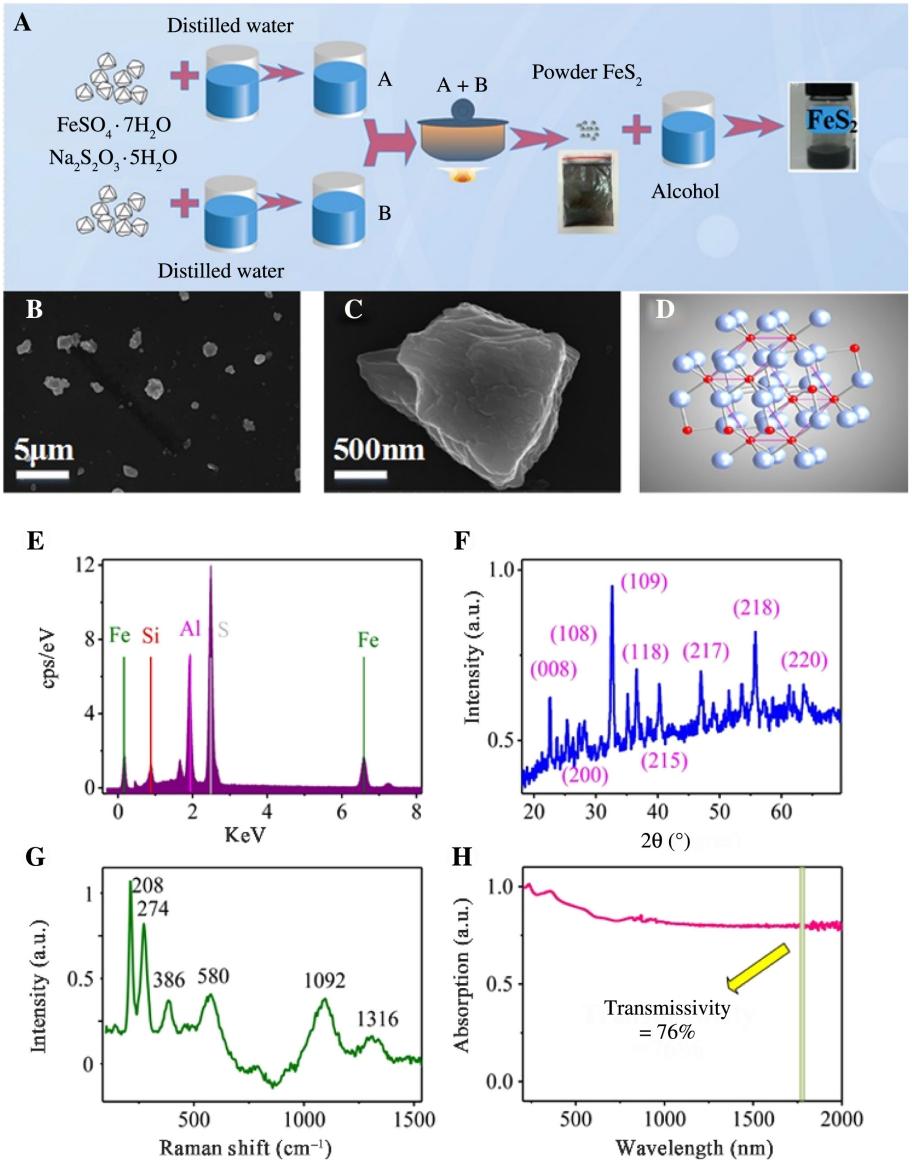

Figure 1: Synthetic procedure and characterization of the layered FeS_2 dispersion.
(A) Schematic illustration of FeS_2 preparation. (B) SEM image with 5 μm scale. (C) SEM image with 500 nm scale. (D) Atomic structure of FeS_2 with red spheres representing Fe and grey ones representing S. (E) EDS analysis of the layered FeS_2 dispersion. (F) HRXRD analysis of the layered FeS_2 dispersion. (G) Raman spectrum of the layered FeS_2 dispersion. (H) UV-Vis-NIR absorption of the layered FeS_2 dispersion.

that FeS_2 can be used as SA in intermediate infrared mode-locked fiber lasers. The transmission of the FeS_2 powder at 1562 nm is 76%.

Figure 2A shows the nonlinear-transmittance measuring system of FeS_2 dispersion. The nonlinear transmission curve of FeS_2 is shown in Figure 2B. A double-balanced detection system which contains a mode-locked fiber laser (the output parameters include 1566.2 nm wavelength, 644 fs pulse duration, and 27.4 MHz repetition rate) and a home-made erbium-doped fiber (EDF) amplifier was built. With femtosecond laser pulses passing through 50/50 output coupler (OC), the output power is divided into two parts: one part is based on SA laser pulse power of FeS_2 material, and the other part is the laser pulse power. At the same time, in order to control the incident laser power, the average power of the mode-locked fiber laser is attenuated by reducing the pump power of the amplifier. The power of the pulses propagating directly to output 2 and the power of the pulses propagating through the FeS_2 to output 1 are detected by two power meters. As a result, we got the modulation depth and saturation intensity of the FeS_2 as 4.5% and 17.5 $MW \cdot cm^{-2}$, respectively

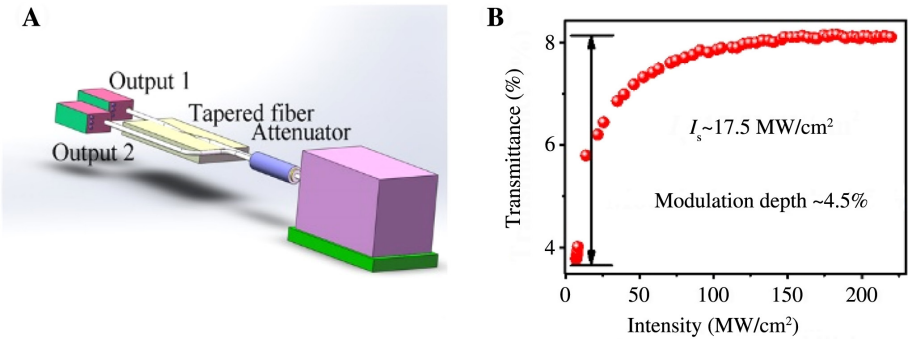

Figure 2: Nonlinear characteristic of FeS_2.
(A) Detecting system for the nonlinear absorbance of FeS_2 dispersion. (B) Nonlinear transmission curve.

3 Results and discussion

Figure 3 shows our experimental setup of the passively mode-locked fiber laser by using FeS_2 as SA. The pump source is a laser diode with 980 nm central wavelength and 423 mW maximum output power. By controlling the current of the pump laser (A_p), the input power of the cavity (P_p) can be manually controlled. The functional dependency of P_p and A_p is $P_p = A_p * 0.74 - 36$. EDF with a length of 1 m (core absorption at 1530 nm is 110 dBm) is used in the cavity to generate 1566.2 nm laser. By applying a polarization-independent isolator, the laser can only propagate in one direction in the cavity to keep the pump laser out of damage. When the three-paddle polarization controller (PC) is not adjusted and mode is not locked, there is only a spike in the pulse and the energy is not enough to make the fiber nonlinear, so self-phase modulation cannot occur to broaden the spectrum, and the light intensity is also absorbed by the SA. When the phase is fixed and the pulse energy is superimposed, high-energy pulse laser enhances the nonlinearity. Thus the self-phase modulation makes the spectrum broaden obviously. At this time, the high-energy laser saturates the absorption of the SA, resulting in ultrashort mode-locking pulses due to pulse width compression. FeS_2 SA is prepared by deposition of FeS_2 microcrystals in the cone region (diameter and length are 13.6 μm and 6 mm, respectively) and doped on the tapered fiber as shown in Figure 3. In the production method of microfiber, the stripped fiber was placed in the internal flame of the flamethrower and slowly stretched outward until the diameter of the fiber reached 13.6 μm to ensure the interaction between the material and evanescent wave of the fiber and to control the loss of the fiber, and then the microfiber is fixed on the optical glass. Based on the optical deposition method of materials, a small amount of FeS_2 is dripped on the microfiber to make the material and fiber fully interact [37]. Compared with the non-deposited tapered fiber, about 41% of the energy is absorbed by FeS_2, which proves that the material is completely in contact with the tapered fiber. Through an optical microscope. The transmission efficiency of the tapered fiber is approximately 86.3%. A 3:7 OC is employed to transfer 70% of the output laser back into the cavity and 30% of the output laser to the detection system. The length of our cavity is approximately 28 m. By using some monitor and record instruments (optical spectrum analyzer [Anritsu MS9710C], 2 GHz photodetector, digital oscilloscope), we can get both the spectral and temporal properties of the mode-locked fiber laser.

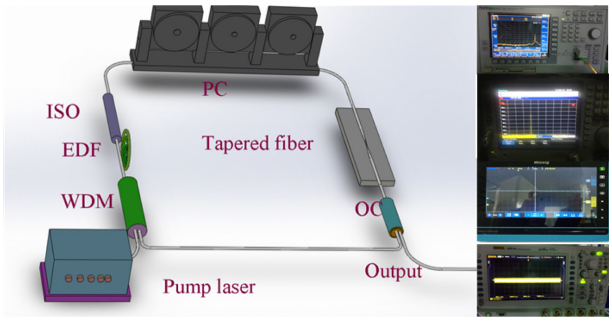

Figure 3: Schematic diagram of the EDF ring laser.
WDM, wavelength division multiplex; EDF, Er-doped fiber; PI-ISO, polarization-independent isolator; PC, polarization controller; OC, output coupler.

In the experiment, mode-locked fiber laser was observed when the pump power is 423 mW and the PC is fixed at an appropriate state. Figure 4A shows the typical spectrum of fiber laser with a center wavelength of 1566.5 nm in which the spectral width is about 2.5 nm. Spectral Kelly sideband is observed here which indicates that our fiber laser operates in the conventional soliton mode-locking regime [38]. Figure 4B shows the pulse train with a period of 162 ns. The inset of Figure 4B is the pulse train with 2 μs span which indicates the stable

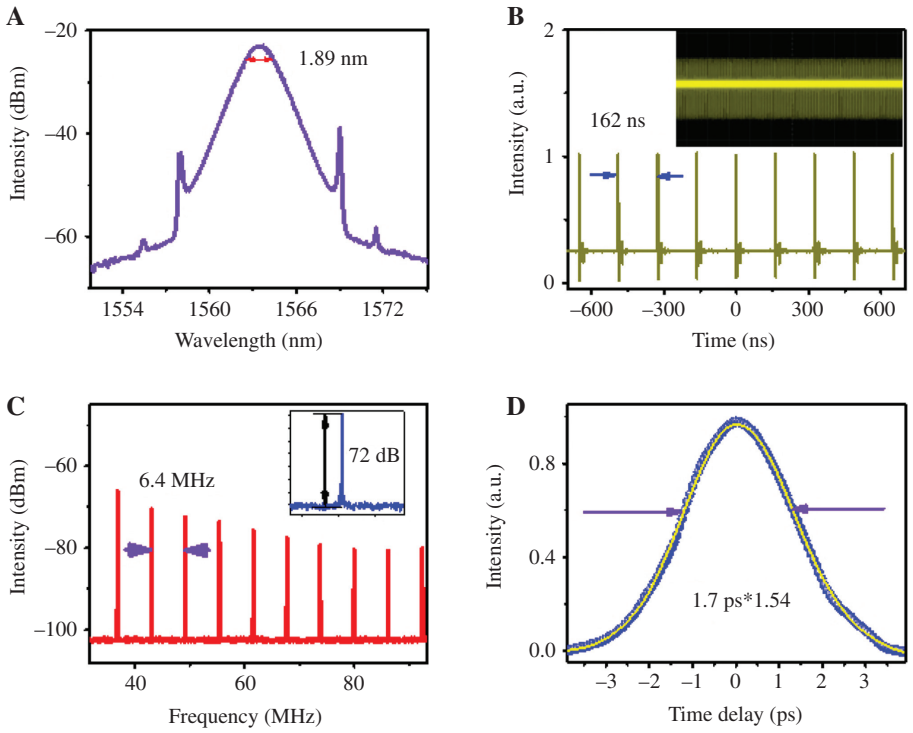

Figure 4: The output characteristics of Er-doped mode-locked fiber laser at the fundamental repetition rate.
(A) Output spectrum; (B) output pulse train at range of 1400 ns, the inset is in the range of 2 μs; (C) RF spectrum of the mode-locked pulses, inset: the broadband RF spectrum; (D) autocorrelation trace with a $sech^2$ fitting.

mode-locking state. The radio frequency (RF) spectrum with a repetition rate of 6.4 MHz and 10 frequency peaks is shown in Figure 4C. The SNR is about 72 dB as shown in the inset of Figure 4C, which means that the influence of interaction between the birefringence effect of the fiber and the nonlinear optical effect of the pulse is unavoidable. Figure 4D shows the autocorrelation traces. According to the fit to a squared hyperbolic secant ($sech^2$) pulse shape, the pulse duration is estimated to be 1.7 ps. The laser cavity can maintain a stable state for more than a week without pulse splitting when the mode locking phenomenon occurs. The output characteristics of typical materials are summarized in Table 1. FeS_2 has obvious advantages as an SA compared with these materials, and this is the first time that FeS_2 is applied to ultrafast photonics. We will further optimize the output parameters of FeS_2 in future studies.

The interaction of optical solitons can be affected by periodically filtering effect which leads to the changes of separation and phase difference of neighboring solitons [44]. Bound states of solitons are known as high-order soliton solutions of the nonlinear Schrodinger equation [45] and the complex Ginzburg-Landau equation [46]. Mode-locked lasers can generate such bound solitons, which have attracted significant interests. With different pulse separation and phase difference under certain situations, different bound states could be supported by different intracavity gain, loss, dispersion, and nonlinearity. Figure 5A shows the experiment results of bound state solitons in which the period of the spectral modulation

Table 1: Output characteristics of erbium-doped mode-locked lasers based on different nonlinear optical materials.

Material	Wavelength (nm)	Pulse width (ps)	Repeat frequency (MHz)	Modulation depth (%)	Refs.
G nanosheets	1557.56	15.7	3.33	\	[39]
MoS_2 film	1595	2.5	1.3	4.4	[40]
BP film	1558	2.18	15.59	\	[41]
$MoSe_2$ nanosheets	1558.25	1.45	61.5	0.63	[42]
MoS_2 nanosheets	1558	3	8.028	10.61	[43]
FeS_2	1566.5	1.7	6.4	4.5	This work

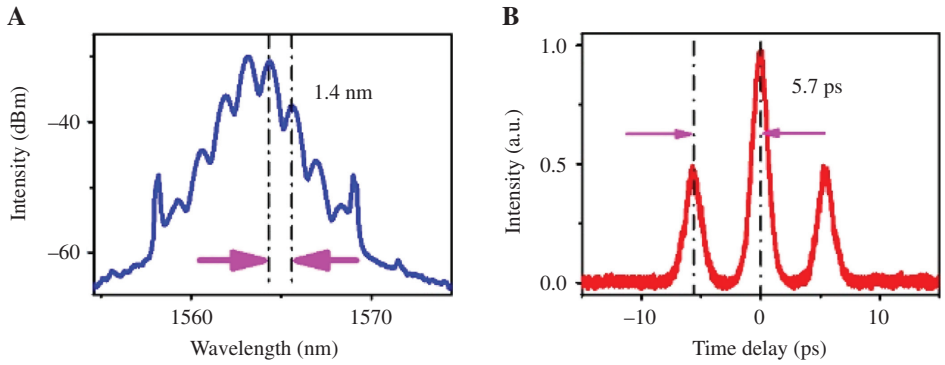

Figure 5: The output of bound state solitons.
(A) The pulse train; (B) the autocorrelation trace.

fringe of the bound state solitons is about $\Delta\nu = \Delta\lambda\nu/\lambda$ in which $\Delta\lambda = 1.4$ nm. Figure 5B shows the autocorrelation trace of the state solitons with the pump power fixed at 316 mW and the PC fixed at appropriate condition. Once the bound states of two solitons are obtained, their soliton separation always falls into one of the three solitons separation values, which indicates that the bound states of solitons have fixed discrete solitons separation. According to the autocorrelation trace shown in Figure 5B, the pulse is a second-order bound soliton. The pulse duration is 2 ps, and the time interval of two autocorrelation traces peaks is about 5.7 ps, which fits well with the calculated result according to $\Delta f = c \cdot \Delta\lambda/\lambda^2$ [38]. The height ratio of the three peaks is 1:2:1. The mechanism of the formation of the bound state solitons is explained as a result of direct soliton interaction [47].

With the pump power increasing, the evolutions of the pulse train, spectrum, and 3-dB width of the spectrum are investigated. Figure 6A shows the spectrum evolution with the pump power of 136, 186, 236, 286, 336, 386 and 436 mW from Figure 6A (B–H, representing the specific pump power value) [43]. The conventional Kelly

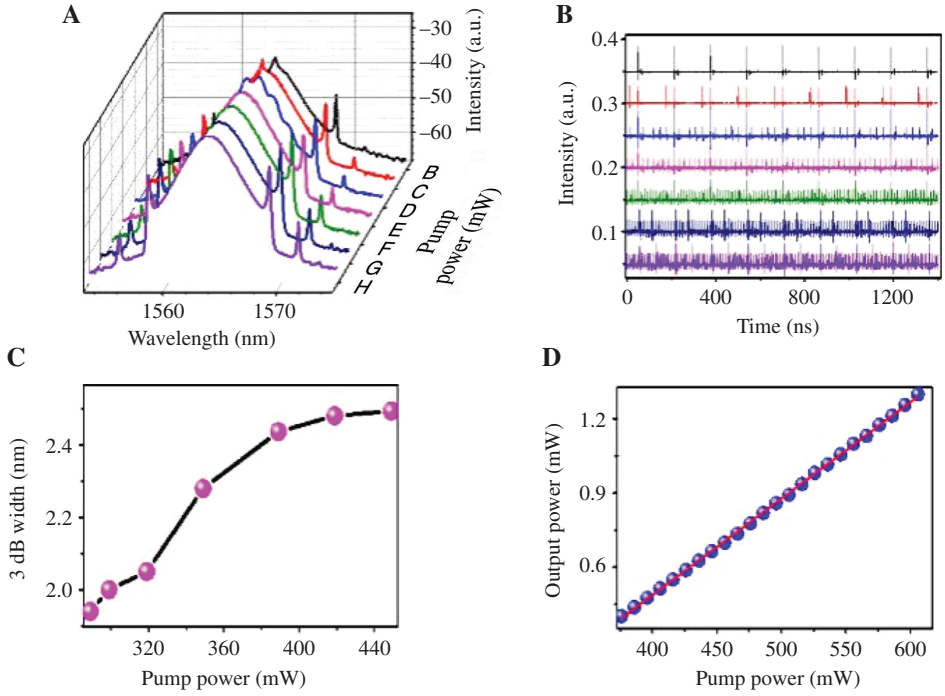

Figure 6: Output signals with the power of the pump increasing.
(A) The spectrum evolution versus the pump power. (B) The pulse train evolution versus the pump power. (C) The 3-dB spectral width versus the pump power. (D) Output power and linear fitting slope curve versus pump power.

sidebands in the spectrum is increasing with the continuously increasing pump power [38]. It appears as continuous waves when the pump power is weak enough as shown in Figure 6A (B and C). Figure 6B shows the pulse trains corresponding to Figure 6A. The pump power is increasing from top to bottom. Mode locking state can be partially explained by the soliton energy quantization theory, due to the soliton energy relocation and the interaction between the multiple solitons per round cavity round trip [48]. When the pump power is 136 mW, the pulse train is on basic frequency. One can clearly see that the pulse trains are splitting from top to bottom with the pump power increasing. When the pump power is high enough, the multiples will form a special state in the fiber cavity. The 3-dB width of the spectra is investigated as shown in Figure 6C; with the increase of pump power, the width of 3 dBm increased from 1.93 nm to 2.46 nm. As the nonlinearity of the fiber increases with the pump power the self-phase modulation leads to further broadening of the spectrum, while the influence of pumping power on the spectral bandwidth decreases when dispersion and nonlinearity accumulation reach a new balance. The influence of pump source on laser can be minimized by choosing proper pump power. The output power increases linearly with the increase of pump current, as shown in Figure 6D in which the dotted line is the experimental result and the solid line is the fitting result.

4 Conclusion

In summary, we experimentally realize a passively mode-locked EDFL by using metal dichalcogenides FeS_2 as SA. The pulse duration of the mode-locked fiber laser is 1.7 ps with the central wavelength of 1563 nm. The modulation depth and saturation intensity are about 4.5% and 17.5 MW cm^{-2}. Both single pulse and bound state solitons can be realized as well as the evolution between them by continuously adjusting the pump power. This work demonstrates that FeS_2 dispersion can be used as a new excellent material for SA photonics and optical modulator which is cheap and convenient.

Acknowledgments: This research was supported by the National Natural Science Foundation of China (61605106); funded projects for the Academic Leader and Academic Backbones, Shaanxi Normal University (18QNGG006); Starting Grants of Shaanxi Normal University (grant number 1112010209, 1110010717); Fundamental Research Funds for the Central Universities (GK201802006, 2018CSLY005); and Open Research Fund of State Key Laboratory of Transient Optics and Photonics, Chinese Academy of Sciences (number SKLST201809, SKLST201401). Funder Name: Open Fund of State Key Laboratory of Information Photonics and Optical Communications (Beijing University of Posts and Telecommunications), P.R. China, Grant Number: IPOC2017B012. Funder Name: Open Research Fund of State Key Laboratory of Pulsed Power Laser Technology, Electronic Engineering Institute, Grant Number: SKL2017KF02.

References

[1] Li X, Wu K, Sun Z, et al. Single-wall carbon nanotubes and graphene oxide-based saturable absorbers for low phase noise mode-locked fiber lasers. Sci Rep 2016;6:25266.
[2] Liu Y, Liu C, Wang X, et al. Photoresponsivity of an all-semimetal heterostructure based on graphene and WTe_2. Sci Rep 2018;8:12840.
[3] Martinez A, Al Araimi M, Dmitriev A, et al. Low-loss saturable absorbers based on tapered fibers embedded in carbon nanotube/polymer composites. APL Photonics 2017;2:126103.
[4] Chernysheva M, Rozhin A, Fedotov Y, et al. Carbon nanotubes for ultrafast fibre lasers. Nanophotonics 2017;6:1–30.
[5] Razak NN, Latiff AA, Zakaria Z, et al. Q-switched erbium-doped fiber laser with a black phosphorus saturable absorber. Photonics Lett Pol 2017;9:72–4.
[6] Wu L, Dong Y, Zhao J, et al. Kerr nonlinearity in 2D graphdiyne for passive photonic diodes. Adv Mater 2019;31:1807981.
[7] Luo M, Fan T, Zhou Y, et al. 2D black phosphorus-based biomedical applications. Adv Funct Mater 2019;29:1808306.
[8] Wu L, Huang W, Wang Y, et al. 2D tellurium based high-performance all-optical nonlinear photonic devices. Adv Funct Mater 2019;29:1806346.
[9] Xie Z, Xing C, Huang W, Zhang H. Ultrathin 2D nonlayered tellurium nanosheets: facile liquid-phase exfoliation, characterization, and photoresponse with high performance and enhanced stability. Adv Funct Mater 2018;28:1705833.
[10] Hui Z, Xu W, Li X, et al. Cu_2S nanosheets for ultrashort pulse generation in the near-infrared region. Nanoscale 2019;11:6045–51.
[11] Zhang Y, Li X, Qyyum A, et al. PbS nanoparticles for ultrashort pulse generation in optical communication region. Part Part Syst Char 2018;35:1800341.
[12] Liu JS, Li XH, Qyyum A, et al. Fe_3O_4 nanoparticles as a saturable absorber for giant chirped pulse generation. Beilstein J Nanotech 2019;10:1065–72.
[13] Guo J, Huang D, Zhang Y, et al. 2D GeP as a novel broadband nonlinear optical material for ultrafast photonics. Laser Photonics Rev 2019;13:1900123.
[14] Ruppert C, Aslan OB, Heinz TF. Optical properties and band gap of single-and few-layer $MoTe_2$ crystals. Nano Lett 2014;14:6231–6.
[15] Liu J, Jiang X, Zhang R, et al. MXene – enabled electrochemical microfluidic biosensor: applications toward multicomponent

continuous monitoring in whole blood. Adv Funct Mater 2019;29:1807326.
[16] Liu H, Luo AP, Wang FZ, et al. Femtosecond pulse erbium-doped fiber laser by a few-layer MoS_2 saturable absorber. Opt Lett 2014;39:4591–4.
[17] Liu M, Zheng XW, Qi YL, et al. Microfiber-based few-layer MoS_2 saturable absorber for 2.5 GHz passively harmonic mode-locked fiber laser. Opt Express 2014;22:22841–6.
[18] Zhang H, Lu SB, Zheng J, et al. Molybdenum disulfide (MoS_2) as a broadband saturable absorber for ultra-fast photonics. Opt Express 2014;22:7249–60.
[19] Kataura H, Kumazawa Y, Maniwa Y, et al. Optical properties of single-wall carbon nanotubes. Synthetic Met 1999;103:2555–8.
[20] Bi C, Yuan Y, Zhang R, et al. A dynamic mode decomposition based edge detection method for art images. IEEE Photonics J 2017;9:1–13.
[21] Aiub EJ, Steinberg D, Thoroh de Souza EA, Saito LAM. 200-fs mode-locked erbium-doped fiber laser by using mechanically exfoliated MoS_2 saturable absorber onto D-shaped optical fiber. Opt Express 2017;25:10546–52.
[22] Alivisatos AP. Semiconductor clusters, nanocrystals, and quantum dots[J]. Sci 1996;271:933–7.
[23] Ennaoui A, Fiechter S, Jaegermann W, Tributsch H. Photoelectrochemistry of highly quantum efficient single-crystalline n-FeS_2 (pyrite). J Electrochem Soc 1986;133:97–106.
[24] Smestad G, Ennaoui A, Fiechter S, et al. Photoactive thin film semiconducting iron pyrite prepared by sulfurization of iron oxides. Sol Energ Mater 1990;20:149–65.
[25] Kim TB, Choi JW, Ryu HS, et al. Electrochemical properties of sodium/pyrite battery at room temperature. J Power Sources 2007;174:1275–8.
[26] Walter M, Zünd T, Kovalenko MV. Pyrite (FeS_2) nanocrystals as inexpensive high-performance lithium-ion cathode and sodium-ion anode materials. Nanoscale 2015;7:9158–63.
[27] Wang ZQ, Nithyanandan K, Coillet A, et al. Optical soliton molecular complexes in a passively mode-locked fibre laser. Nat Commun 2019;10:830.
[28] Hamdi S, Coillet A, Grelu P. Real-time characterization of optical soliton molecule dynamics in an ultrafast thulium fiber laser. Opt Lett 2018;43:4965–8.
[29] Bonaccorso F, Sun Z, Hasan T, et al. Graphene photonics and optoelectronics. Nat Photonics 2010;4:611.
[30] Wang F, Rozhin AG, Scardaci V, et al. Wideband-tuneable, nanotube mode-locked, fibre laser. Nat Nanotech 2008;3:738–42.
[31] Zhou KG, Zhao M, Chang MJ, et al. Size-dependent nonlinear optical properties of atomically thin transition metal dichalcogenide nanosheets. Small 2015;11:694–701.
[32] Zhang M, Wu Q, Zhang F, et al. 2D black phosphorus saturable absorbers for ultrafast photonics. Adv Opt Mater 2019;7:1800224.
[33] Chai T, Li X, Feng T, et al. Few-layer bismuthene for ultrashort pulse generation in a dissipative system based on an evanescent field. Nanoscale 2018;10:17617–22.
[34] Li X, Yu X, Sun Z, et al. High-power graphene mode-locked Tm/Ho co-doped fiber laser with evanescent field interaction. Sci Rep 2015;5:16624.
[35] Yu X, Yu P, Wu D, et al. Atomically thin noble metal dichalcogenide: a broadband mid-infrared semiconductor. Nat Commun 2018;9:1545.
[36] Yu X, Li Y, Hu X, et al. Narrow bandgap oxide nanoparticles coupled with graphene for high performance mid-infrared photodetection. Nat Commun 2018;9:4299.
[37] Zeng C, Liu X, Yun L. Bidirectional fiber soliton laser mode-locked by single-wall carbon nanotubes. Opt Express 2013;21:18937–42.
[38] Zhang Y, Li X, Qyyum A, Feng T, Guo P, Jiang J. PbS nanoparticles for ultrashort pulse generation in optical communication region. Part Part Syst Char 2018;35:1800341.
[39] Wang J, Luo Z, Zhou M, et al. Evanescent-light deposition of graphene onto tapered fibers for passive Q-switch and mode-locker. IEEE Photonics J 2012;4:1295–305.
[40] Cui Y, Lu F, Liu X. MoS_2-clad microfibre laser delivering conventional, dispersion-managed and dissipative solitons. Sci Rep 2016;6:1–8.
[41] Park K, Lee J, Lee YT, et al. Black phosphorus saturable absorber for ultrafast mode-locked pulse laser via evanescent field interaction. Ann Phys 2015;527:770–6.
[42] Luo Z, Li Y, Zhong M, et al. Nonlinear optical absorption of few-layer molybdenum diselenide ($MoSe_2$) for passively modelocked soliton fiber laser. Photonics Res 2015;3:A79–86.
[43] Du J, Wang Q, Jiang G, et al. Ytterbium-doped fiber laser passively mode locked by few-layer molybdenum disulfide (MoS_2) saturable absorber functioned with evanescent field interaction. Sci Rep 2014;4:6346.
[44] Akhmediev NN, Ankiewicz A, Soto-Crespo JM. Multisoliton solutions of the complex Ginzburg-Landau equation. Phys Rev Lett 1997;79:4047.
[45] Tratnik MV, Sipe JE. Bound solitary waves in a birefringent optical fiber. Phys Rev A 1988;38:2001.
[46] Malomed BA. Bound solitons in the nonlinear Schrödinger/Ginzburg-Landau equation. In: Fournier JD, Sulem PL. (eds). Large Scale Structures in Nonlinear Physics. Lecture Notes in Physics, Vol. 392. Springer, Berlin, Heidelberg, 1991:288–94.
[47] Wu X, Tang DY, Luan XN, et al. Bound states of solitons in a fiber laser mode locked with carbon nanotube saturable absorber. Opt Commun 2011;284:3615–8.
[48] Loh KP, Bao QL, Eda G, Chhowalla M. Graphene oxide as a chemically tunable platform for optical applications. Nat Chem 2010;2:1015–24.